Oxygen Diffusion in $YBa_2Cu_3O_{7-\delta}$ Studied via $^{133}Ba(EC)^{133}Cs$ Nuclear Quadrupole Interaction*

W. Tröger and T. Butz

Physik-Department, Technische Universität München, D-8046 Garching, Germany

Z. Naturforsch. **47a**, 12–20 (1992); received August 9, 1991

The oxygen diffusion in $YBa_2Cu_3O_{7-\delta}$ was studied between 300 K and 1273 K in flowing oxygen by monitoring the $^{133}Ba(EC)^{133}Cs$ nuclear quadrupole interaction by time differential perturbed angular correlation. The data are analyzed in a model of two different nearest neighbour oxygen configurations and yield hopping rates, the energy barrier and the difference in free enthalpy between both states. In addition, we studied the reduced system $YBa_2Cu_3O_{6+\varepsilon}$.

1. Introduction

The oxygen diffusion in the high-T_c superconductor $YBa_2Cu_3O_{7-\delta}$ has been studied extensively in the past by bulk techniques applied to powder samples. On the contrary, local techniques like hyperfine techniques thus far either addressed static aspects of the Cu-environment [1] or were carried out on samples doped with impurity probes [2]. In this paper we report on the first measurements of the $^{133}Ba(EC)^{133}Cs$ nuclear quadrupole interaction (NQI) in $YBa_2Cu_3O_{7-\delta}$ by time differential perturbed angular correlation (TDPAC). We deduce hopping rates for the mobile oxygen as well as energy barriers representative for the elementary jump process. The extraction of such information from macroscopic measurements of bulk diffusion in powder samples is complicated since these also depend on particle size and morphology.

2. Experimental

Samples of $YBa_2Cu_3O_{7-\delta}$, prepared by standard synthesis at the INPG-ENSPG, St. Martin d'Hères, France, were doped with ^{133}Ba. They exhibited a sharp transition to the superconducting state at 94 K as detected by their AC-susceptibility. $YBa_2Cu_3O_{6+\varepsilon}$ was produced from $YBa_2Cu_3O_{7-\delta}$ by keeping the sample at 1023 K under a stream of Ar at 1 atm for 24 hours. After completion of the TDPAC measurements this sample was reoxidized to $YBa_2Cu_3O_{7-\delta}$. Since ^{133}Ba is not a very favourable TDPAC isotope (small anisotropy $A_{22}^{\text{eff}}=3\%$, short halflife of the $I=5/2^+$ intermediate state of the 365 keV – 81 keV γ–γ-cascade) the high efficiency Munich TDPAC setup [3] was used. A miniature, water-cooled furnace (22 mm outer diameter) allowed to heat the sample up to 1273 K under a steady flow of oxygen or argon at 1 atm (see Figure 1). Typically, we collected data for two or three days with $0.5-1\cdot10^9$ coincidence counts. This extreme statistical accuracy and the observation of the correlation out to ten times $t_{1/2}$ were absolutely necessary in order to derive details of the NQI, e.g. asymmetry parameters or line broadening.

* Presented at the XIth International Symposium on Nuclear Quadrupole Resonance Spectroscopy, London, United Kingdom, July 15–19, 1991.

Reprint requests to Dr. T. Butz, Physik-Department, Technische Universität München, W-8046 Garching, FRG.

3. Results

3.1. $YBa_2Cu_3O_{6+\varepsilon}$ and $YBa_2Cu_3O_{7-\delta}$ at 300 K

The room temperature spectra of the $^{133}Ba(EC)^{133}Cs$ NQI in $YBa_2Cu_3O_{6+\varepsilon}$ and $YBa_2Cu_3O_{7-\delta}$ are shown in Fig. 2, top and bottom, respectively. All spectra exhibit a baseline shift which is probably due to selfabsorption in the sample. The spectrum for $YBa_2Cu_3O_{6+\varepsilon}$ exhibits axial symmetry ($\eta=0$), whereas the spectrum for $YBa_2Cu_3O_{7-\delta}$ has $\eta=0.41(5)$. This is in qualitative agreement with the results obtained by NQR on $^{135,137}Ba$ [4]. From Fig. 2 it is also clear that the precession frequency in $YBa_2Cu_3O_{7-\delta}$ ($\omega=97(2)$ Mrad/s) is larger than for $YBa_2Cu_3O_{6+\varepsilon}$ ($\omega=71(1)$ Mrad/s). However, this difference is essentially due to the asymmetry parameter difference; for $\nu_Q=e^2qQ/h$ with $eq=V_{zz}$ denoting the largest component of the electric field gradient (EFG) tensor and Q being the nuclear quadrupole moment

0932-0784 / 92 / 0100-0012 $ 01.30/0. – Please order a reprint rather than making your own copy.

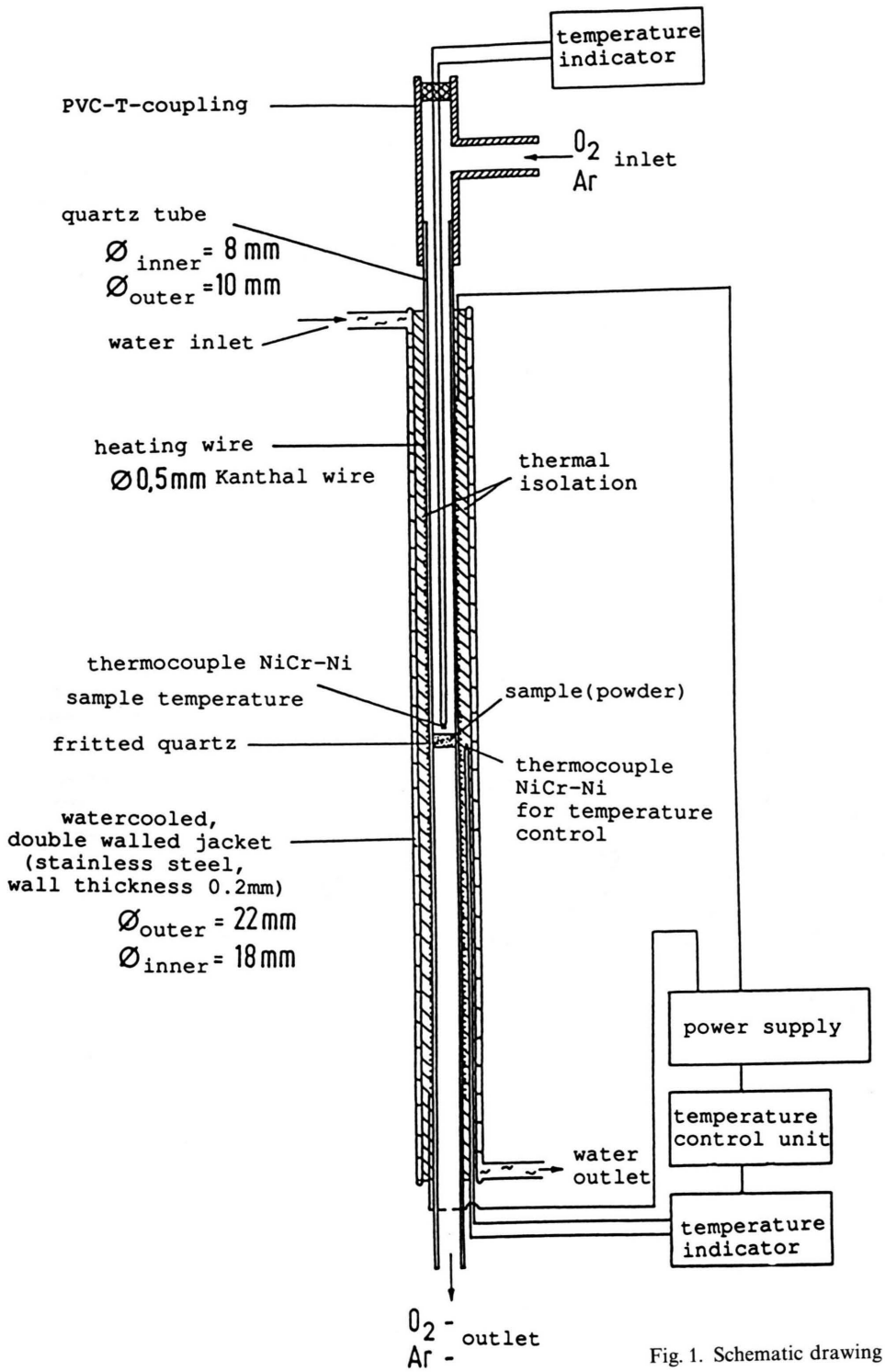

Fig. 1. Schematic drawing of the miniature furnace.

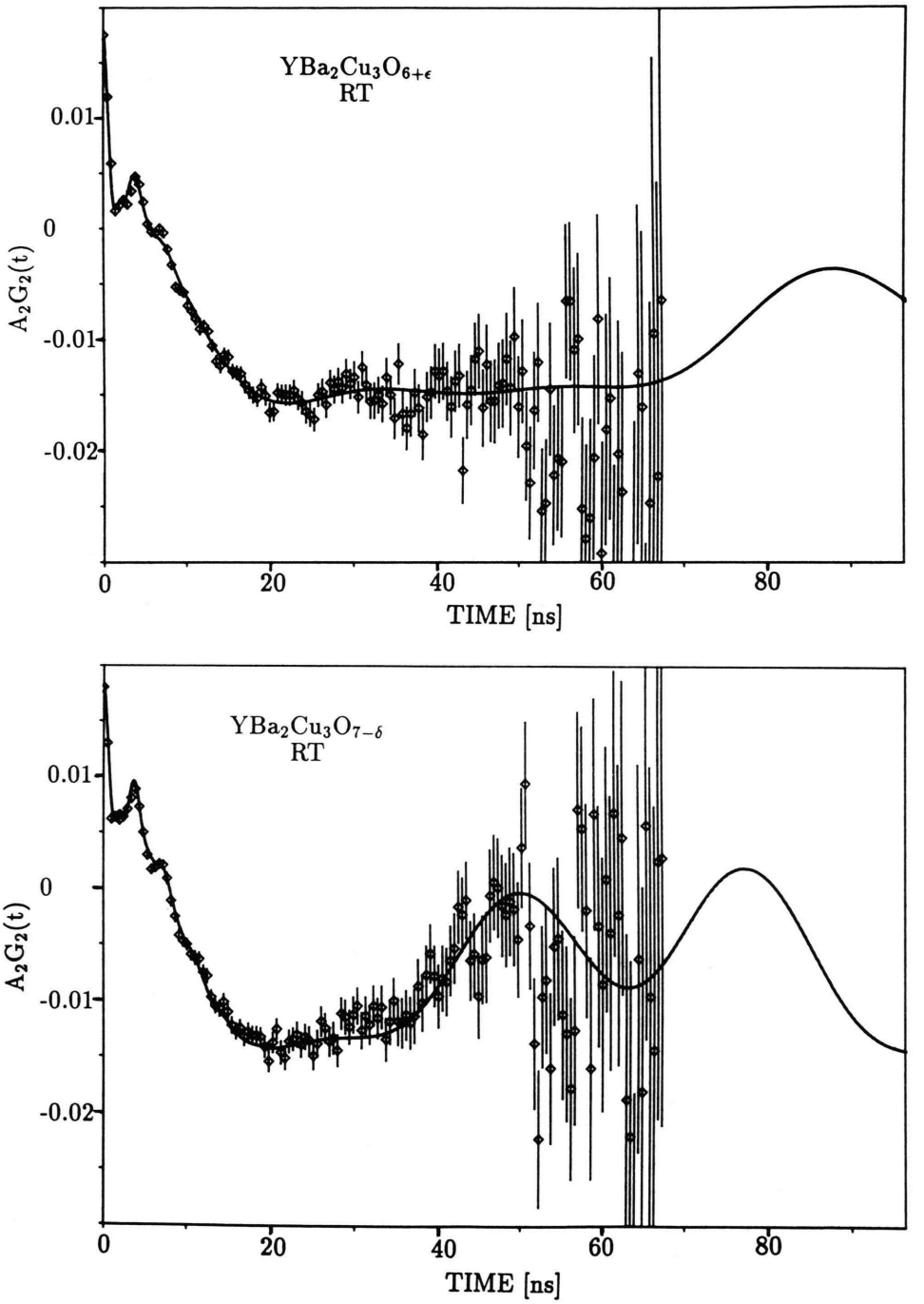

Fig. 2. TDPAC spectrum of the $^{133}Ba(EC)^{133}Cs$ NQI at room temperature in $YBa_2Cu_3O_{6+\varepsilon}$ (top) and in $YBa_2Cu_3O_{7-\delta}$ (bottom).

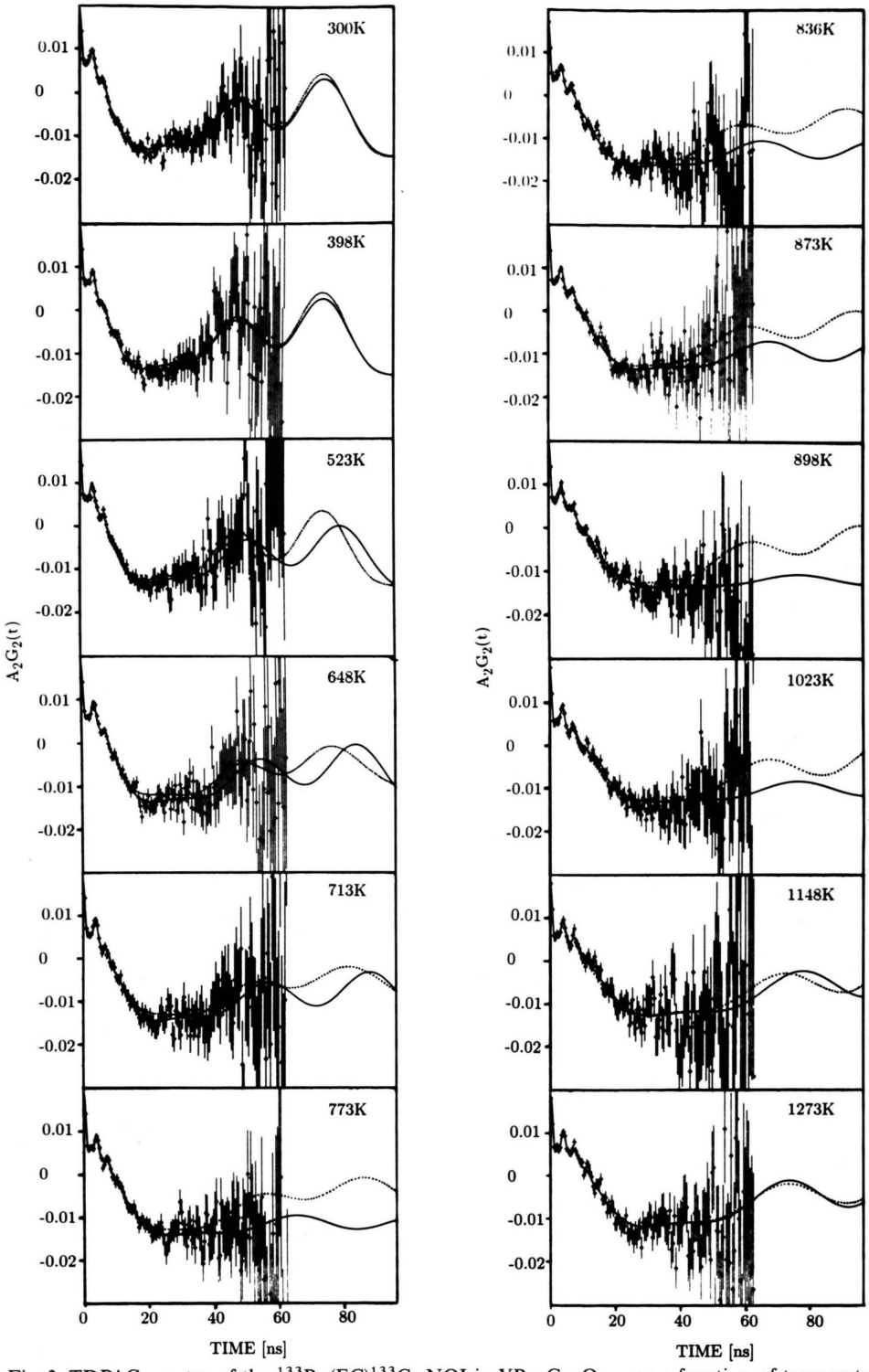

Fig. 3. TDPAC spectra of the $^{133}Ba(EC)^{133}Cs$ NQI in $YBa_2Cu_3O_{7-\delta}$ as a function of temperature. The sample was kept under a stream of oxygen at 1 atm during heating. The solid line is the result of a least squares fitting analysis using the function of (1) (slow relaxation model). The dotted line is the result of the *simultaneous* fit of the two-state model (see appendix).

of the $I=5/2^+$ state ($Q=0.22(5)$ b) we have

$$\nu_Q = 88(5)\ \text{MHz} \quad \text{and} \quad \nu_Q = 75(1)\ \text{MHz}$$

for $YBa_2Cu_3O_{7-\delta}$ and $YBa_2Cu_3O_{6+\varepsilon}$, respectively.

After reoxidation of $YBa_2Cu_3O_{6+\varepsilon}$ to $YBa_2Cu_3O_{7-\delta}$ we obtained essentially the same parameters as those obtained previously before reduction.

Another feature which is clearly visible in Fig. 2 is the high frequency component with $\omega \approx 1.65$ Mrad/s superimposed onto the slow quadrupole precession pattern. This component is present in both samples. It is rather strongly damped and disappears between 10 ns and 20 ns.

3.2. Temperature Dependence of the NQI in $YBa_2Cu_3O_{7-\delta}$

The TDPAC spectra for the $^{133}Ba(EC)^{133}Cs$ NQI in $YBa_2Cu_3O_{7-\delta}$ under 1 atm oxygen flow are shown in Fig. 3 for the temperature range from 300 K up to 1273 K. The solid and the dotted lines are two different fitting curves as will be described below. It is clear from this figure that the NQI decreases with increasing temperature. At higher temperatures it becomes increasingly more difficult to determine the asymmetry. parameter. In order to avoid the rather strong correlation between the fitted precession frequency ω and the asymmetry parameter η at high temperatures we decided to keep η fixed at $\eta=0.41$ over the entire temperature range. A first approach to analyze the data was to fit the following perturbation function to the spectra:

$$G_2(t) = e^{-\lambda_C t} \cdot G_2^{\text{static}}(t)\,. \tag{1}$$

Here,

$$G_2^{\text{static}}(t) = 0.229 + 0.339 \cdot \cos(\omega t) + 0.284 \cdot \cos(1.65\,\omega t) + 0.148 \cdot \cos(2.65\,\omega t)$$

and λ_C is the relaxation parameter introduced in the approximation of the Blume's Stochastic model by Baudry and Boyer [5]. In fact, for technical reasons we fitted the sum of λ_C and $\lambda_N = 1/\tau_N$, the lifetime of the $I=5/2^+$ state. In addition we included a high frequency component with $\omega=1.65$ Grad/s, $\delta=0.15$ of the form (we call it magnetic for reasons discussed below)

$$G_2^{\text{magnetic}}(t) = 0.2 + 0.4\,e^{-\delta\omega t}\cos(\omega t) + 0.4\,e^{-2\delta\omega t}\cos(2\omega t). \tag{2}$$

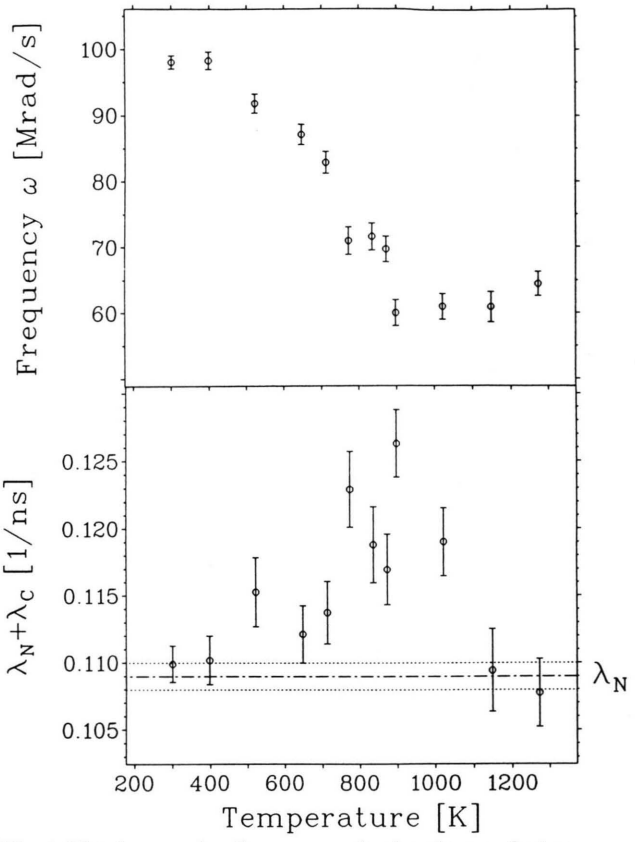

Fig. 4. Fitted precession frequency ω (top) and sum of relaxation and nuclear decay constant $\lambda_C+\lambda_N$ versus temperature (bottom) for the analysis proposed by Baudry and Boyer [5]. The dashed-dotted line is λ_N with the dotted lines indicating the error limits of λ_N.

The frequency, the damping δ (or linebroadening) and the fraction of the magnetic contribution were all found to be constant over the entire temperature range.

The results of the individual least squares fitting analysis of all 12 spectra is shown in Fig. 4. The precession frequency ω changes considerably from close to 100 Mrad/s to about 60 Mrad/s at temperatures above 900 K (see Fig. 4, top). This decrease of ω is accompanied by an increase of λ_C (see Fig. 4, bottom) from about zero at 300 K to values around 0.015 ns^{-1} in the temperature range around 800 K to 900 K and a subsequent decrease again to zero at the highest temperatures. The zero λ_C is characteristic for a static NQI at 300 K; the increase of λ_C is typical for a fluctuating EFG – superimposed to a static contribution – at intermediate temperatures; the final decrease of λ_C to zero is a sign for complete motional narrowing at the highest temperatures. In principle it should be

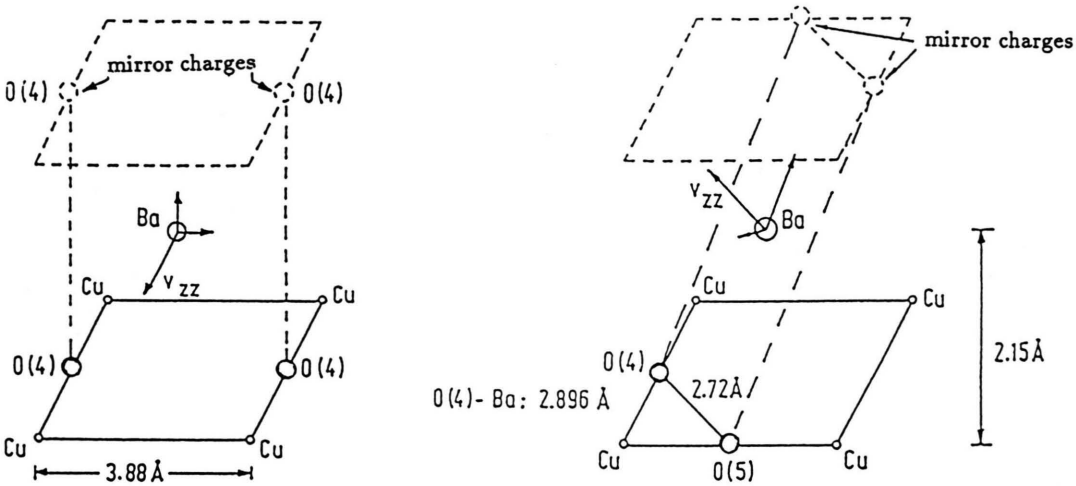

Fig. 5. Position of oxygen in the state I (left) on O(4)-sites and in the state II (right) on the neighbouring O(4)- and O(5)-sites.

possible to derive hopping rates from a $\ln \lambda_C$ vs. $1/T$ plot as discussed in [5]. However, the accuracy of the present data is not sufficient to render such an approach meaningful. Therefore we adopted a different procedure. Rather than to fit each spectrum individually we performed a least squares fitting analysis of all 12 spectra *simultaneously* with five non-trivial parameters. The model used is rather simple: we assumed a two state model with state I at 300 K having ω_I, separated by a barrier of ΔE from the second state II with ω_{II} which has a free enthalpy difference ΔG compared to state I. The hopping rates re

$$\gamma_I = \gamma_0 \cdot e^{-\Delta E/k_B T} \quad \text{and} \quad \gamma_{II} = \gamma_0 \cdot e^{-(\Delta E - \Delta G)/k_B T}. \qquad (3)$$

In this way, the progressive decrease of the average precession frequency as well as the increase in linewidth at intermediate temperatures, and the motional averaging at high temperatures can all be modelled *simultaneously* for a suitable set of parameters γ_0, ΔE, ΔG, ω_I, and ω_{II}. In our model, we assumed that the EFG fluctuates in magnitude only without a noticeable reorientation. This follows from the observation that our baseline – although always too low because of selfabsorption in the sample – was essentially constant. The resulting perturbation function is derived in the appendix.

From the simultaneous fit we obtained

$\gamma_0 = 560(90)\ \text{ns}^{-1}$, $\omega_I = 97.5(7)$ Mrad/s,

$\Delta E = 555(18)$ meV, $\omega_{II} = -79(9)$ Mrad/s.

$\Delta G = 145(6)$ Mrad/s,

The quality of the two-state model fit was about the same as for the Baudry-Boyer model (1), but required 5 parameters only compared to 24 in the latter case.

4. Discussion

4.1. Temperature Dependence of the NQI in $YBa_2Cu_3O_{7-\delta}$

The observed temperature variation of the NQI parameters ω and λ_C is characteristic for systems with fluctuating EFG's, e.g. due to diffusing oxygen. In particular, the strong decrease of ω with temperature is unlikely to be the result of lattice expansion alone. Moreover, the characteristic increase of λ_C at low temperatures followed by a decrease at high temperatures points directly to fluctuating EFG's due to the oxygen diffusion and would be unexplainable in a static picture.

In order to extract more information from the two-state model analysis we have to associate specific near neighbour configurations of the $^{133}Ba(EC)^{133}Cs$ probe with these states. We identify state I with the oxygen on O(4) positions ("trans-position"), as shown in Fig. 5 (left), and state II with oxygen residing on neighbouring O(4)- and O(5)-sites, as shown in Fig. 5 (right). The EFG arising from these two oxygen atoms (we include in Fig. 5 the mirror charges of these atoms to facilitate the derivation of the EFG orientation) has to be added tensorially to the EFG arising from all the other charges. A crude approximation for the

latter would be the EFG in $YBa_2Cu_3O_{6+\varepsilon}$ with V_{zz} along the crystal c-axis. This identification of states with specific oxygen configurations is suggested by the work of Jorgenson et al. [6] who proposed that the orthorhombic-to-tetragonal phase transition in $YBa_2Cu_3O_{7-\delta}$ is of the order-disorder type. The mobile oxygen atoms are the O(4) and O(5) atoms.

We are now in a position to identify the parameters derived from the two-state analysis with a specific hopping process: the O(4) oxygen atom in the trans-configuration attempts to jump onto the energetically less favourable position O(5) about 600 times per nanosecond (this is close to typical lattice vibration frequencies); although the difference in free enthalpy is comparatively low, the barrier is very high such that these jumps are not very probable and the population of state II remains low even at high temperatures. At present, we do not know why we see no discontinuous features at the orthorhombic-to-tetragonal phase transition near 973 K. Possibly, the fact that the spectroscopy is actually performed on ^{133}Cs, obtained by electron capture from ^{133}Ba, is responsible for this phenomenon. A similar argument was given by Singh et al. [2] for their studies using ^{111}In as a probe. Contrary to their experiment, however, we see an unbroadened, static signal at low temperatures, which progressively broadens at intermediate temperatures, and enters the motional narrowing regime at very high temperatures. We have no explanation for the fact that the ^{111}In spectra of Singh et al. [2] showed massive linebroadening at the lowest temperature and exhibited motional narrowing right away from 250 K upwards. Therefore, we can not identify their activation energy of 33(4) meV for oxygen jumps with any of our derived quantities. Probably, as outlined by Singh et al. [2], the near neighbour oxygen O(4) to Cu(1) is not mobile for In on a Cu(1) site.

There are some points of criticism for the simple two-state model analysis. First, the existence of configuration II implies that the neighbouring unit cell has a configuration with three oxygen atoms on O(4), O(5), and O(4) sites. Since this process is thermally activated and can also take place before the nuclear transformation from ^{133}Ba to ^{133}Cs, we should in principle include this third configuration in our analysis. After the transmutation, we might – of course – have a completely different scenario of possible oxygen configurations. Secondly, we certainly lose a certain amount of oxygen, even under 1 atm of flowing oxygen, at temperatures over 900 K [6]. Thus, the implicit assumption of constant stoichiometry in the two-state model is not correct.

4.2. Origin of the High Frequency Component

The high frequency component which is visible in all spectra is believed to be much too high to be of quadrupolar origin. We have observed this component with two different spectrometers (fast-slow and slow-fast principle). Moreover, the same component was observed by P. Vulliet at Grenoble [7] with yet another spectrometer. Therefore, we exclude trivial problems with the electronics as a possible explanation. We rather think that it originates from the electron capture process in the ^{133}Ba-decay: the Cs atom could remain in a state with a p-hole left over after the rearrangement of the electronic shell. This p-hole could lead to a magnetic field of the order of 300 kG [8] which is close to what we observe. However, we certainly do not see the perturbation pattern of the free atom hyperfine interaction. Wether our approach (2) is correct or not is difficult to decide regarding the rather strong damping of the oscillation. In any case, we believe that a hole in the Cs shell is responsible for the high frequency component. Admittedly, the lifetime of this hole configuration is rather long for a conducting material. The Ba-environment must be considered "insulating" with the Ba–O polyhedra being the skeleton only and being completely separated spatially from the conducting electron pathways and unaffected by the onset of superconductivity. In fact, no anomalies were observed in the $^{133}Ba(EC)^{133}Cs$ NQI in $EuBa_2Cu_3O_{7-\delta}$ [9]. This parallels the fact that Y can be substituted by almost any rare earth without affecting T_C.

Acknowledgement

We gratefully acknowledge the continuous interest and support of this work by Prof. Dr. G. M. Kalvius. It is a pleasure to thank Dr. J. P. Senateur and Dr. F. Weiss, INPG-ENSPG, St. Martin D-Hères, France, for the preparation and Dr. P. Vulliet, CEN Grenoble, for the loan of the sample.

Appendix

The two-state diagonal motional narrowing formulae in the frequency domain are given in any standard textbook, e.g. [10]. Here, we derive the perturbation function in the time domain.

We require the matrix elements of the operator

$$\hat{\Omega}(t)=e^{\begin{pmatrix}-3i(m^2-m'^2)\,\omega_Q^{I}-\gamma_I & \gamma_I \\ \gamma_{II} & -3i(m^2-m'^2)\,\omega_Q^{II}-\gamma_{II}\end{pmatrix}t}. \tag{4}$$

Using the operator identity

$$e^{\hat{A}}=e^{a_0}\left(\hat{E}\cosh a+\frac{\boldsymbol{a}\boldsymbol{\sigma}}{a}\sinh a\right) \tag{5}$$

with

$$\hat{A}=\hat{E}a_0+\boldsymbol{a}\boldsymbol{\sigma},\quad \boldsymbol{a}=\begin{pmatrix}a_x\\a_y\\a_z\end{pmatrix},\quad a=\sqrt{a_x^2+a_y^2+a_z^2}$$

and the Pauli Spin matrices

$$\boldsymbol{\sigma}=\begin{pmatrix}\sigma_x\\\sigma_y\\\sigma_z\end{pmatrix},\quad \sigma_x=\begin{pmatrix}0&1\\1&0\end{pmatrix},\quad \sigma_y=\begin{pmatrix}0&-i\\i&0\end{pmatrix},\quad \sigma_z=\begin{pmatrix}1&0\\0&-1\end{pmatrix},$$

we arrive at

$$a_0=iz\bar{\omega}-\bar{\gamma},\quad \alpha_x=\bar{\gamma},\quad a_y=i\Delta\gamma,\qquad a_z=iz\Delta\omega-\Delta\gamma \tag{6}$$

with

$$\bar{\gamma}=\frac{\gamma_I+\gamma_{II}}{2},\quad \Delta\gamma=\frac{\gamma_I-\gamma_{II}}{2},\quad z=-3(m^2-m'^2),\quad \bar{\omega}=\frac{\omega_Q^{I}+\omega_Q^{II}}{2},\quad \Delta\omega=\frac{\omega_Q^{I}-\omega_Q^{II}}{2}.$$

This yields finally

$$\hat{\Omega}(t)=e^{-\bar{\gamma}t+iz\bar{\omega}t}\begin{pmatrix}\cosh(at)+\dfrac{iz\Delta\omega-\Delta\gamma}{a}\sinh(at) & \dfrac{\gamma_I}{a}\sinh(at)\\ \dfrac{\gamma_{II}}{a}\sinh(at) & \cosh(at)-\dfrac{iz\Delta\omega-\Delta\gamma}{a}\sinh(at)\end{pmatrix}. \tag{7}$$

Assuming detailed balance $P_I\cdot\gamma_I=P_{II}\cdot\gamma_{II}$ with P_I and P_{II} denoting the population of state I and II (with $P_I+P_{II}=1$), we arrive at

$$\sum_{I,II}P_I\langle I|\,\hat{\Omega}(t)\,|II\rangle=e^{-\bar{\gamma}t+iz\bar{\omega}t}\left[\cosh(at)+\left(\bar{\gamma}-\frac{iz(\Delta\omega)(\Delta\gamma)}{\bar{\gamma}}\right)\frac{\sinh(at)}{a}\right]. \tag{8}$$

This expression replaces the usual static expression e^{izwt}.

The limiting cases are:

a) $\bar{\gamma}\to 0,\ \dfrac{\Delta\gamma}{\bar{\gamma}}\to 0$: $\quad \frac{1}{2}(e^{iz\omega_I t}+e^{iz\omega_{II}t})$ "*static superposition*",

b) $\bar{\gamma}^2\gg z^2\Delta\omega^2,\ \bar{\gamma}\gg z\Delta\omega\Delta\gamma$: $\quad e^{iz\bar{\omega}t}$ "*complete motional narrowing*".

In the case of axial symmetry the perturbation function $G_{kk}(t)$ is now the sum over all m, m' values of (8) multiplied with the usual intensities $\begin{pmatrix}I & I & k\\ m' & -m & p\end{pmatrix}^2$.

Note, that the hardcore remains unaffected because for $z=0$ (8) reduces to unity. The expression for $G_{kk}(t)$ is real because replacing z by $-z$ in (8) yields the complex conjugate. For non-axial symmetry (but constant asymmetry parameter η) we have to sum over $\Delta\omega_j(\eta)$ and $\bar{\omega}_j(\eta)$ and over the proper intensities for the given η.

[1] Y. Kohori, H. Shibai, Y. Oda, Y. Kitaoka, T. Kohara, and K. Asayama, J. Phys. Soc. Japan **57,** 1568 (1988).
[2] P. Singh, M. N. Nyayate, S. H. Devare, and H. G. Devare, Phys. Rev. **B 39,** 2308 (1989).
[3] T. Butz, S. Saibene, T. Fraenzke, and M. Weber, Nucl. Instrum. Meth. **A 284,** 417 (1989).
[4] H. Lüttgemeier, Hyp. Int. **61,** 1051 (1990).
[5] A. Baudry and P. Boyer, Hyp. Int. **35,** 803 (1987).
[6] J. D. Jorgensen, M. A. Beno, D. G. Hinks, L. Soderholm, K. J. Volin, R. L. Hitterman, J. D. Grace, I. K. Schuller, C. U. Segre, K. Zhang, and M. S. Kleefisch, Phys. Rev. **B 36,** 3608 (1987).
[7] P. Vulliet, private communication.
[8] H. Kopfermann, Kernmomente, 2. Aufl., Akad. Verlagsgesellschaft m.b.H., Frankfurt a. M. 1956.
[9] W. Tröger, P. Vulliet, J. P. Senateur, F. Weiss, T. Butz, and A. A. Lerf, Hyp. Int. **61,** 1151 (1990).
[10] A. Abragam, The Principles of Nuclear Magnetism, Clarendon Press, Oxford 1961.